HHS Public Access

Author manuscript

Neuroimage. Author manuscript; available in PMC 2019 January 01.

Published in final edited form as:

Neuroimage. 2018 January 01; 164: 59–66. doi:10.1016/j.neuroimage.2016.12.063.

Hemifield columns co-opt ocular dominance column structure in human achiasma

Cheryl A. Olman[1], **Pinglei Bao**[2], **Stephen A. Engel**[1], **Andrea Grant**[3], **Chris Purington**[4], **Cheng Qiu**[5], **Michael-Paul Schallmo**[6], and **Bosco S. Tjan**[7]

[1]Department of Psychology, University of Minnesota, Minneapolis, MN

[2]Department of Biology and Biological Engineering, California Institute of Technology, Pasadena, CA

[3]Department of Neuroscience, University of Minnesota, Minneapolis, MN

[4]University of California, Berkeley, Berkeley, CA

[5]Schepens Eye Research Institute, Harvard Medical School, Boston, MA

[6]Department of Psychology, University of Washington, Seattle, WA

[7]Department of Psychology, University of Southern California, Los Angeles, CA

Abstract

In the absence of an optic chiasm, visual input to the right eye is represented in primary visual cortex (V1) in the right hemisphere, while visual input to the left eye activates V1 in the left hemisphere. Retinotopic mapping In V1 reveals that in each hemishphere left and right visual hemifield representations are overlaid (Hoffmann et al., 2012). To explain how overlapping hemifield representations in V1 do not impair vision, we tested the hypothesis that visual projections from nasal and temporal retina create interdigitated left and right visual hemifield representations in V1, similar to the ocular dominance columns observed in neurotypical subjects (Victor et al., 2000). We used high-resolution fMRI at 7T to measure the spatial distribution of responses to left- and right-hemifield stimulation in one achiasmic subject. T_2-weighted 2D Spin Echo images were acquired at 0.8 mm isotropic resolution. The left eye was occluded. To the right eye, a presentation of flickering checkerboards alternated between the left and right visual fields in a blocked stimulus design. The participant performed a demanding orientation-discrimination task at fixation. A general linear model was used to estimate the preference of voxels in V1 to left- and right-hemifield stimulation. The spatial distribution of voxels with significant preference for each hemifield showed interdigitated clusters which densely packed V1 in the right hemisphere. The spatial distribution of hemifield-preference voxels in the achiasmic subject was stable between two days of testing and comparable in scale to that of human ocular dominance columns. These results are the first *in vivo* evidence showing that visual hemifield representations interdigitate in

achiasmic V1 following a similar developmental course to that of ocular dominance columns in V1 with intact optic chiasm.

Introduction

A congenital condition known as achiasma or non-decussating retinal-fugal fiber syndrome results in a failure of axons from retinal ganglion cells on the nasal side of the retina to cross to the contralateral side of the brain (Apkarian et al., 1994; Apkarian et al., 1995). The result is the absence of an optic chiasm, with all projections from the right eye following a path through the right lateral geniculate nucleus (LGN) to the right primary visual cortex (V1), and all projections from the left eye going to left V1 (Victor et al., 2000; Williams et al., 1994a). Functional mapping studies show that these projections are functional, and the entire visual field (all information being received from each eye) is represented in each hemisphere (Davies-Thompson et al., 2013; Hoffmann et al., 2012; Kaule et al., 2014). Crucially, retinotopic mapping studies reveal that representations of the two halves of the visual field, which are separated between the two hemispheres in the neurotypical visual system, are superimposed on each other in the visual cortex of an achiasmic individual (Hoffmann et al., 2012) but functionally independent (Bao et al., 2015).

The fact that achiasmic individuals have functional vision and can readily discriminate objects in mirror-symmetric locations in the visual field indicates that left and right visual field representations are not confused in visual cortex, in spite of their complete overlap. The most likely explanation is that the left and right visual field representations are interdigitated in primary visual cortex, co-opting the mechanisms that typically guide left and right eye projections to cortex. In achiasmic Belgian sheep dogs, Williams et al. (1994) found that axons from nasal retina that should have crossed at the optic chiasm are targeted to different layers in the LGN than axons from temporal retina (so left- and right-hemifield layers replace ipsi- and contra-lateral eye layers in the LGN). In a study of achiasma in humans, Victor et al. (2000) hypothesized that if axons from separate layers in the LGN follow typical developmental markers then they should segregate in the input layers of V1.

To examine this hypothesis that inputs from left- and right-hemifleld locations are segregated in the primary visual cortex of an achiasmic individual, we performed T_2-weighted functional MRI with 0.8 mm (isotropic) resolution. The prediction under our hypothesis is that the functional imaging would reveal alternating stripes of left- and right-hemifield dominance in V1 that were observed in the same cortical location on separate days.

Methods

Participants

One participant with achiasma (male, age 31) and two control participants (one male, age 26, and one female, age 43) each participated in two separate scanning sessions after providing written informed consent. The experimental protocol was approved by the University of Minnesota Institutional Review Board. The participants had previously

participated in other scanning sessions to acquire T_1-weighted anatomical images and retinotopic mapping data. The retinotopic mapping data for the achiasmic participant (reported in (Bao et al., 2015)) confirmed that mirror symmetric points in the visual field map to apparently identical locations in each hemisphere of primary visual cortex.

Visual stimulus and task for achiasmic participant

Visual stimuli consisted of black and white flickering checkerboards (spatial frequency: 0.5 cycles/degree; temporal frequency: 2 Hz) presented via an Avotec Silent Vision Fiber Optic Glasses (Avotec Inc., Stuart FL) to the participant's right eye. The left eye was covered with a patch for comfort, so the participant could relax both eyes during the scanning session.

Each scan consisted of 8 checkerboard presentation blocks, 4 in the left visual field and 4 in the right visual field. Total visual field subtense was 24° (w) x 18° (h). Each presentation block lasted 12 sec and was followed by 12 sec of rest. Including an additional rest block at the beginning of the scan, every scan was 208 sec long. Stimulus presentation order was not randomized, and always alternated between hemifields, starting with the left in each scan. A total of 12 scans were conducted in "Day 1", and were repeated in "Day 2".

During each scan, the participant's attention was engaged by a demanding orientation discrimination task on the fixation mark in the center of the screen. At random intervals uniformly distributed between 2 and 6 sec, the fixation mark randomly changed from '+' to '×' for about 400 ms before returning to '+'. The x could be slightly tilted 5 deg either in clockwise or counterclockwise direction. The participant had to report, by pressing one of two buttons, the direction of tilt as soon as the change was detected.

Visual stimulus and task for control experiments

Two normally sighted control participants were also recruited. The visual stimulus and task were identical *except* presentation was always in one hemifield and alternated between eyes.

Functional Imaging

Functional MRI data were collected at the University of Minnesota's Center for Magnetic Resonance Research on a Siemens 7 Tesla scanner equipped with the AC-84 head-gradient insert, which has a maximum strength of 80 mT/m and a slew rate of 333 T/m/s. A custom-made radio frequency head coil (4-channel transmit, 9-channel receive; Adriany et al., 2012) was used for T_2-weighted (spin echo) echo-planar imaging (EPI) in the achiasmic participant and the first of the two control participants. Images were acquired with a coronal field of view (FOV) in 24 slices (0.8 mm thick) positioned near the occipital pole (Figure 1). Nominal image resolution was 0.8 mm isotropic (field of view: 152x114 mm; matrix size: 192x144); data were acquired with an in-plane parallel imaging acceleration factor (R) of 2 and a right-left phase-encode direction (6/8 Partial Fourier, echo-spacing: 0.8 ms). The repetition time (TR) was 2.0 sec. At the end of each scanning session, a 30-volume EPI series was acquired with a left-right phase-encode direction (reversed from the phase-encode direction of the functional data acquisition) to assist in distortion compensation during data processing. Scanning parameters were identical for the second control participant, except a

newly available 4-channel transmit, 32-channel receive coil was used, enabling greater acceleration (R=3) to combat distortion, albeit at the cost of signal-to-noise ratio.

Anatomical data processing

Cortical surfaces (gray matter/white matter boundary, and pial surface) were determined from a standard 1-mm isotropic T_1-weighted MP-RAGE reference anatomy using FreeSurfer (https://surfer.nmr.mgh.harvard.edu/). No manual editing was done to adjust the surfaces. Visual inspection confirmed that the gray matter (GM) delineation was reasonable in the region of the calcarine sulcus.

Data pre-processing

Functional data were analyzed using tools provided by AFNI (https://afni.nimh.nih.gov/afni). Functional data were preprocessed in three steps: motion compensation (6-parameter affine transformation), distortion compensation (non-linear transformation), and non-linear warping to the reference anatomy. Transformation matrices or warping maps were saved from each step and then combined to resample the original data to a pre-processed dataset in a single step.

First, motion compensation was performed using `3dvolreg`, using the mean of the (motion-compensated) last scan of the scanning session as the reference toward which other scans were corrected. Next, distortion compensation was performed using the -plusminus option in `3dQwarp`, using the PE-reversed EPI acquisition to generate a WARP volume that could compensate distortions caused by field distortions in the scanner. The reference T_1-weighted anatomical image was then registered to the unwarped EPI dataset, using `3dAllineate`, the *lpc* cost function, and a weighting function that was a binary mask of the mean EPI image from the entire scanning session.

Finally, a second stage of nonlinear distortion compensation was performed, again using `3dQwarp`, but this time seeking a non-linear WARP volume that would register the EPI to the T_1-weighted anatomical image from which cortex GM labels and GM depths would be derived. This step was not performed until a very good EPI-anatomical registration was accomplished (using `3dAllineate`) after the initial round of distortion compensation. The EPI were used as the base dataset, so a weight matrix could be used in this `3dQwarp` step that was a combination of three things: a binary mask derived from the EPI data, a blurred weighting function derived from pericalcarine GM and WM anatomical labels, and a smoothed voxel displacement map that decreased the weight for regions of the EPI image where field perturbations were large. While it may seem redundant to do 2 stages of non-linear warping (`3dQwarp` with the PE-reversed scan, and then `3dQwarp` to the anatomy), we found that nonlinear warping between the EPI and the reference anatomy without first compensating for known distortions was an under-constrained problem that produced nonsensical solutions (judged by visual inspection and with a metric that considered an alignment “good” when it maximized the percentage of visually responsive voxels that were localized to GM vs. WM). Because the EPI data were used as the base dataset in this step, it was actually the inverse of this WARP volume that was combined with the previous WARP volume (from PE-reversed distortion compensation) and the motion compensation

parameters to resample the original EPI data into a data set optimized for registration to the reference anatomy.

During the second scanning session ("Day 2") for the achiasmic participant, equipment errors occurred and the participant needed to be removed from the scanner half-way through the scanning session. Therefore, the first 6 and second 6 scans were acquired separately, with separate distortions and slightly different slice placement. To accommodate this, the scans were analyzed separately (motion compensation, distortion compensation, and then warping to the reference anatomy), and then a between-session alignment matrix was estimated by registering the functional data from the second scanning session to the first. This between-session registration matrix was then applied to the second (partial) scanning session to sample it into the space of the first, creating a complete 12-scan dataset to compare against the "Day 1" dataset.

Data analysis

Data were processed with a standard GLM (`3dDeconvolve`, including Legendre polynomials and motion parameter estimates as nuisance regressors) to estimate the amplitude of response to left and right hemifield stimuli (percent signal change) via linear regression against a model that was a boxcar function convolved with a gamma function. For each voxel, the full-model F statistic was used to assess significance of the response in that voxel, and two metrics were then derived for further analysis.

Sensitivity was defined as the average response to visual stimulus (sensitivity = (|L|+|R|)/2). This metric was used to assess responsivity of the gray matter throughout the cortical depth, to ensure that the T_2-weighted imaging had mitigated the contributions of large pial vessels to the signal. *Selectivity* was defined as the difference in responses to left- and right-hemifield stimuli, divided by the average response (selectivity = (L-R)/sensitivity). This is the metric that was used to map responses and inspect the data for column-like structures once it was visualized on the cortical surface.

To assess responses across the cortical surface and through the depth of the GM, the `3dVol2Surf` function of SUMA (https://afni.nimh.nih.gov/afni/suma) was used to resample to 7 "depths" spanning the cortical thickness. This depth-sampling has a resolution of 0.3–0.4 mm, more than twice the nominal resolution of our data. A similar resampling was also done across the cortical surface for the visualizations (below). In both cases, sampling the data at a finer resolution than was acquired was done only for visualization purposes, and not to imply that the data had resolution better than their nominal resolution of 0.8 mm. For each functional data parameter (significance, sensitivity and selectivity) the result of this `3dVol2Surf` resampling step was a list of 7 values spanning the cortical depth for each surface vertex in the cortex. Because the sampling extended into the WM and beyond the pial surface by 20% of the local cortical depth, the first and last surfaces were discarded from further analysis, and only the 5 depths contained in the GM were used.

Data visualization

To create flattened representations of the cortical surface for visualization of data, patches of the inflated cortical surface containing just the calcarine sulcus were manually cut in FreeSurfer's `tksurfer` tool and flattened using FreeSurfer's `mris_flatten` tool. The mean distance between neighboring vertices on the flattened cortical surface was 0.6 mm. For each vertex contained in the calcarine sulcus patch, values of significance, selectivity and sensitivity were then assigned to an appropriate location in the three-dimensional space defined by the flattened patch and the depth-dependent volume sampling done by `3dVol2Surf`. For visualization, the data at each depth were re-gridded to a regular grid with spacing of 0.5 mm using Python (`scipy.interpolate.griddata`).

Results

One achiasmic individual participated in two days of scanning sessions, each session consisting of 12 3 ½-minute scans during which checkerboard stimuli were presented in alternating 12-sec blocks (with rest in between) to the left and right visual field of the right eye. Our slice prescription covered a portion of the calcarine sulcus; slice prescription on the two days was close to identical in the anterior-posterior dimension (i.e., coverage was almost identical, Fig. 2). Maps of regions showing significant modulation across the 12 scans and throughout the cortical depth ($F_{2,1199} > 4.609$, $p < 0.01$ at the single-voxel level) revealed a region on the upper bank of the calcarine sulcus where visual responses were strong and registration between functional and anatomical data was excellent on both days. Further analyses were focused on this region (white boxes, Fig. 2). Both inclusion criteria (functional activation strength and EPI/T_1 registration) contributed to the exclusion of data on the lower bank of the calcarine sulcus from further analysis. This is due in large part to the fact that this particular individual's right-hemisphere calcarine sulcus is very close to the ventral surface of the cortex, where field perturbations by the sagittal and transverse sinuses and bone-tissue interfaces are greatest. Two control participants also completed two scanning sessions each, and their data were processed in the same way as the achiasmic participant's data. Results from these participants are provided as supplementary figures.

To confirm that the T_2-weighted data acquisition was minimizing contributions to the signal from large surface veins, known to degrade resolution, we computed sensitivity profiles through the cortical depth in the regions where significant modulation throughout the cortical depth indicated good registration between functional and anatomical data. The sensitivity profiles in Fig. 3, left panel, show the expected peak response amplitude near the top of the parenchyma (De Martino et al., 2013; Goense and Logothetis, 2006; Koopmans et al., 2010). The selectivity of the signal for left vs. right hemifield (or eye, in the case of the control participants) is flat through the cortical depth (Fig. 3, right panel). Selectivity is expected to be maximal in the middle of the parenchyma, for all participants because spatial selectivity is best for the small vessels in the middle of the gray matter and for normally-sighted individuals because segregation of LGN inputs in neurotypical human is greatest in middle layers. While our nominal imaging resolution was 0.8 mm, blurring due to brain motion, head motion, and T_2* blurring due to the relatively long read-out time of the functional data acquisition decrease the resolution of this experiment. Therefore, our true

resolution is likely 1 mm or above, and inadequate for detecting signals unique to middle layers.

Distribution of preference for left versus right visual hemifield stimulation across the V1 cortical surface is visualized at multiple sampling depths in Fig. 4. On both days, regions were observed where stripes of left-hemifield preference alternated with stripes of right-hemifield preference. These stripes were close to 1 mm wide (average width of one full left/right cycle was 2.5 mm), which is comparable to the widths of ocular dominance columns observed in humans (Cheng et al., 2001; Goodyear and Menon, 2001; Nasr et al., 2016; Yacoub et al., 2007). Importantly, the stripes were observed in the same locations on each day. In the top panels of Fig. 5, data sampled from the middle of the cortical depth on each day are shown side by side with fiducial marks (black lines) in the same location on the cortical surface to illustrate the consistency of the locations of left-hemisphere-dominated responses.

In spite of careful work to compensate for distortion in the EPI data and maximize accuracy of the image registration in the calcarine sulcus, residual errors in alignment are apparent in the fact that the most striking alternation between left- and right-hemifield dominance was observed at slightly different depths across the region of V1 selected for analysis. This is understandable, since the region being analyzed spans several centimeters across the cortical surface, including sections of high positive curvature on the bank of the calcarine sulcus and regions of strong negative curvature, so very small residual distortions in errors in image registration result in an apparent change in the depth of functional data.

To facilitate visualization, a composite image was created by selecting regions of the data from each depth showing strong structure at 2–3 cycles/mm (the expected alternation frequency of ocular or hemifield dominance columns) across the cortical surface and then merging them into a single visualization. To accomplish this, a roving window (~1 cm^2) was used to assign each cortical location a value representing the power in the 2–3 cycles/mm band (a donut, in Fourier space) relative to the entire Fourier transform of the selectivity data in the 1 cm^2 window centered on that location. The power map at each depth was then raised to the 8^{th} power and used as a weighting function for combining the images shown in Fig. 4 to create the composite images shown in the bottom panels of Fig. 5. No image filtering was done. Stripes at this scale were already prominent in different depth samples before the data were aggregated (Fig. 4); spatial frequency content was simply used as a weighting function to determine the relative weight of the selectivity patterns at each depth for each location, to aid visualization.

Comparable figures for the control participants (single-depth ocular dominance maps and through-depth composite images) are included in the supplemental material. Because of the low selectivity for eye-of-origin in the control participants, the maps were not nearly as clear as for the achiasmic participant. Where visible, the alternating-eye structure had the same spatial scale (1 cycle every 2–3 mm) as observed for hemifield alternation in the achiasmic participant.

Discussion

We found that the cortical representation of the left and right visual hemifield of an achiasmic human participant are interdigitated in V1 in the form of hemifield dominance columns, co-opting the structure of ocular dominance in neurotypical V1. This finding, while unprecedented, is broadly anticipated. Prior to our current finding, it has been observed that both hemifields from each eye of achiasmic humans are fully represented in the brain hemisphere ipsilateral to the eye (Bao et al., 2015; Davies-Thompson et al.; Hoffmann et al., 2012; Kaule et al., 2014; Victor et al., 2000; Williams et al. 1994). Detailed retinotopic mappings (Bao et al., 2015; Hoffmann et al., 2012; Kaule et al., 2014) further revealed that visual field locations symmetrically positioned across the vertical meridian are represented by the same cortical locations in the retinotopically defined visual areas at a coarse resolution resolvable with 2–3 mm isotropic voxels. Despite the apparent retinotopic overlap, a broad range of psychophysical and physiological measurements have failed to show any interaction between the left and right visual fields (Bao et al., 2015; Victor et al., 2000). Williams et al. (1994) found in achiasmic Belgian sheep dog that inputs from the two visual fields stay segregated in the LGN, with layers for inputs from the contralateral eyes reassigned to inputs from the ipsilateral visual field, although the same study did not investigate any down-stream structures. These observations have led several authors to hypothesize that the ocular dominance columns in neurotypical V1 may be co-opted to form hemifield dominance columns in achiasma and albinism. (Albinism results in a complimentary condition associated with over-decussating fibers (Bao et al., 2015; Davies-Thompson et al., 2013; Guillery et al., 1984; Hoffmann and Dumoulin, 2015; Victor et al., 2000)). Our finding is the first empirical confirmation of this hypothesis in human.

Bao et al. (2015) had hypothesized that hemifield dominance is maintained downstream from V1 but its spatial organization becomes finely intermingled. They argued that those neurons that would have binocularity in a neurotypical visual system become monocular and unilateral in achiasma by randomly suppressing and pruning one of the inputs, because inputs from the two visual hemifields do not correlate. Since the pruning is random, the resulting spatial distribution of hemifield dominance becomes spatially intermingled downstream from Layer 4 of V1, which receives the segregated inputs from LGN. The depth profile of selectivity we obtained in the current study (Fig. 3) suggests a minor revision to this hypothesis. While selectivity seems to decrease in the superficial layers, indicative of increasing spatial randomness in visual field dominance as suggested by Bao et al., we did not observe the same trend in the deep layers. Selectivity stayed relative constant from middle to deep layers. However, the fact that the depth at which hemifield dominance patterns were strongest fluctuated across the cortical surface due to distortion, even in the small region we had selected, indicates that the depth profiles are likely blurred in this sample, and further studies are required to verify the laminar profile of hemifield selectivity in achiasmic humans.

Recent advances in imaging technology have made it possible to measure millimeter-scale structures in a wide range of participants, including clinical populations. Historically, studies of ocular dominance columns were done with anisotropic sampling resolution, focusing on a flat section of cortex through which a relatively thick slice could be placed to sample across

the cortical surface with sub-millimeter in-plane resolution but poor resolution through the gray matter thickness (Cheng et al., 2001; Yacoub et al., 2007). Studying only planar regions of gray matter is, of course, an unwelcome restriction for neuroscience, particularly when it comes to studying special populations. Multi-channel surface coil arrays with small loops provides the signal-to-noise ratio (SNR) needed for small voxel volumes, and parallel imaging permits single-shot acquisition of large image matrices, thereby enabling multi-slice acquisition with reasonable SNR and temporal resolution.

As isotropic coverage of cortex increases, so does difficulty in registration between functional (EPI) and anatomical (MP-RAGE) data. Distortion compensation techniques, based either on fieldmaps (e.g., FSL's FUGUE) or comparison of EPI acquisitions with opposite phase-encode directions (e.g., FSL's TOPUP or AFNI's 3dQwarp), do mitigate the problem. However, these techniques are not perfect, and even if they were, gradient non-linearities mean that anatomical and EPI scans often have different, sometimes unknown distortions. In the present work, we found that the residual disagreements between EPI and MP-RAGE structure existed on a smaller scale than could be explained by gradient or scanner non-linearities, so we adopted the pragmatic approach of using image-based non-linear warping of the EPI image to match the anatomical image, constraining the unwarping process with a weighting function that emphasized peri-calcarine regions. This additional step improved the image registration 20%, using the ratio of visually modulated voxels aligned with anatomical GM vs WM masks as a metric. The result was adequate for visualization of ocular dominance columns, but inadequate for assessing depth-dependent responses over a significant area of cortex. In the past, we have addressed this problem by restricting our analyses to very limited regions of cortex in which EPI/MP-RAGE registration could be visually verified (Olman et al., 2012). In the future, improved techniques that rely on GM/WM contrast in the EPI data (Kok et al., 2016) will be required to ensure that isotropic sampling resolution translates to reliable estimates of responses across the cortical surface *and* through the GM depth.

The selectivity index we used to assess hemifield dominance in each voxel or at each surface node was typically 10–20% in regions where hemifield dominance patterns were visible. Given our underlying model that inputs are entirely segregated according to hemifield of origin, a 10–20% advantage in the fMRI response is on the low end of expectations. However, the experiment used a single-condition design. In general, studies performed at ultra-high resolution seek to maximize contrast between conditions by adopting a differential design, directly contrasting Condition A and Condition B with no rest in between. These differential designs all but eliminate contributions from large vessels (Olman et al., 2007) and maximize the selectivity of the resulting stimulus. We instead chose a more conservative approach of allowing rest between blocks. This ensured that we were measuring the full hemodynamic response to each hemifield, and not artificially creating contrast between the left- and right-field stimuli. We used a T_2-weighted acquisition to minimize contamination of the signal from the largest veins on the pial surface (Olman and Yacoub, 2011). However, intracortical venuoles with intermediate diameters (~100 μm) that drain cortical territories comparable to the size of an ocular or hemifield dominance column contribute significantly to the T_2-weighted signal. Therefore, blurring by the vascular tree likely diminished the selectivity of the signal measured in each voxel. Participant motion and

brain pulsatility should also blur the signal and reduce voxel selectivity due to partial volume effects. Data smoothness was estimated for the processed functional data (after motion and distortion compensation, as well as warping to anatomy) using AFNI's 3dFWHMx routine. Consistent with previous work (Kemper et al., 2015), smoothness was greatest in the phase-encode direction (σ= 0.9 mm) and least in the through-slice direction (σ = 0.5 mm for through-slice direction, and 0.6 mm for read-out direction). Thus, in spite of our nominal 0.8 mm isotropic resolution, our sampling was blurred in the right/left direction. Lastly, part of the BOLD signal may not be stimulus specific but instead driven by anticipatory responses induced by the blocked timing of the stimulus (Sirotin and Das, 2009). All of these factors likely contributed to selectivity values that were typically 10–20% even for voxels or vertices centered on hemifield dominance columns in the middle of the cortical depth.

While spatial distortions caused by field inhomogeneity and gradient nonlinearities remain the key challenges for imaging fine functional structures at 7T, we were able to reveal columnar structures in the striate cortex of a single individual who does not have a favorably shaped calcarine sulcus. This individual was born without the optic chiasm. Our results constitute the first direct in vivo evidence showing that in human achiasma, the representations of the left and right visual hemifield interdigitate in the striate cortex, co-opting the ocular dominance column in a neurotypical V1.

Supplementary Material

Refer to Web version on PubMed Central for supplementary material.

Acknowledgments

NSF BCS-1255994 and NIH R01 EY017707 to Tjan, NIH R21 EY025731 to Olman, P41 EB015894, P30 N5076408, P30 EY011374, S10 RR026783 and WM KECK Foundation

References

Adriany, G., Waks, M., Tramm, B., Schillak, S., Yacoub, E., DeMartino, F., Van de Moortele, P-F., Naselaris, T., Olman, CA., Vaughan, JT., Ugurbil, K. An open faced 4 ch. loop transmit/16 ch. receive array coil for HiRes fMRI at 7 Tesla. 20th Annual Meeting of the International Society for Magnetic Resonance in Medicine; Melbourne, Australia. 2012.

Apkarian P, Bour L, Barth PG. A unique achiasmatic anomaly detected in non-albinos with misrouted retinal-fugal projections. Eur J Neurosci. 1994; 6:501–507. [PubMed: 8019686]

Apkarian P, Bour LJ, Barth PG, Wenniger-Prick L, Verbeeten B. Non-decussating retinal-fugal fibre syndrome. An inborn achiasmatic malformation associated with visuotopic misrouting, visual evoked potential ipsilateral asymmetry and nystagmus. Brain. 1995; 118(Pt 5):1195–1216. [PubMed: 7496780]

Bao P, Purington CJ, Tjan BS. Using an achiasmic human visual system to quantify the relationship between the fMRI BOLD signal and neural response. Elife. 2015:4.

Cheng K, Waggoner RA, Tanaka K. Human ocular dominance columns as revealed by high-field functional magnetic resonance imaging. Neuron. 2001; 32:359–374. [PubMed: 11684004]

Davies-Thompson J, Scheel M, Jane Lanyon L, Sinclair Barton JJ. Functional organisation of visual pathways in a patient with no optic chiasm. Neuropsychologia. 2013; 51:1260–1272. [PubMed: 23563109]

De Martino F, Zimmermann J, Muckli L, Ugurbil K, Yacoub E, Goebel R. Cortical Depth Dependent Functional Responses in Humans at 7T: Improved Specificity with 3D GRASE. Plos One. 2013:8.

Goense JB, Logothetis NK. Laminar specificity in monkey V1 using high-resolution SE-fMRI. Magn Reson Imaging. 2006; 24:381–392. [PubMed: 16677944]

Goodyear BG, Menon RS. Brief visual stimulation allows mapping of ocular dominance in visual cortex using fMRI. Hum Brain Mapp. 2001; 14:210–217. [PubMed: 11668652]

Guillery RW, Hickey TL, Kaas JH, Felleman DJ, Debruyn EJ, Sparks DL. Abnormal central visual pathways in the brain of an albino green monkey (Cercopithecus aethiops). J Comp Neurol. 1984; 226:165–183. [PubMed: 6330179]

Hoffmann MB, Dumoulin SO. Congenital visual pathway abnormalities: a window onto cortical stability and plasticity. Trends Neurosci. 2015; 38:55–65. [PubMed: 25448619]

Hoffmann MB, Kaule FR, Levin N, Masuda Y, Kumar A, Gottlob I, Horiguchi H, Dougherty RF, Stadler J, Wolynski B, Speck O, Kanowski M, Liao YJ, Wandell BA, Dumoulin SO. Plasticity and stability of the visual system in human achiasma. Neuron. 2012; 75:393–401. [PubMed: 22884323]

Kaule FR, Wolynski B, Gottlob I, Stadler J, Speck O, Kanowski M, Meltendorf S, Behrens-Baumann W, Hoffmann MB. Impact of chiasma opticum malformations on the organization of the human ventral visual cortex. Hum Brain Mapp. 2014; 35:5093–5105. [PubMed: 24771411]

Kemper VG, De Martino F, Vu AT, Poser BA, Feinberg DA, Goebel R, Yacoub E. Sub-millimeter T2 weighted fMRI at 7 T: comparison of 3D-GRASE and 2D SE-EPI. Front Neurosci. 2015; 9:163. [PubMed: 25999810]

Kok P, Bains LJ, van Mourik T, Norris DG, de Lange FP. Selective Activation of the Deep Layers of the Human Primary Visual Cortex by Top-Down Feedback. Curr Biol. 2016; 26:371–376. [PubMed: 26832438]

Koopmans PJ, Barth M, Norris DG. Layer-specific BOLD activation in human V1. Hum Brain Mapp. 2010; 31:1297–1304. [PubMed: 20082333]

Nasr S, Polimeni JR, Tootell RB. Interdigitated Color- and Disparity-Selective Columns within Human Visual Cortical Areas V2 and V3. J Neurosci. 2016; 36:1841–1857. [PubMed: 26865609]

Olman CA, Inati S, Heeger DJ. The effect of large veins on spatial localization with GE BOLD at 3 T: Displacement, not blurring. Neuroimage. 2007; 34:1126–1135. [PubMed: 17157534]

Olman CA, Yacoub E. High-field FMRI for human applications: an overview of spatial resolution and signal specificity. Open Neuroimag J. 2011; 5:74–89. [PubMed: 22216080]

Olman CA, Harel N, Feinberg DA, He S, Zhang P, Ugurbil K, Yacoub E. Layer-specific fMRI reflects different neuronal computations at different depths in human V1. PLoS ONE. 2012; 7(3):e32536. [PubMed: 22448223]

Sirotin YB, Das A. Anticipatory haemodynamic signals in sensory cortex not predicted by local neuronal activity. Nature. 2009; 457:475–479. [PubMed: 19158795]

Victor JD, Apkarian P, Hirsch J, Conte MM, Packard M, Relkin NR, Kim KH, Shapley RM. Visual function and brain organization in non-decussating retinal-fugal fibre syndrome. Cereb Cortex. 2000; 10:2–22. [PubMed: 10639391]

Williams RW, Hogan D, Garraghty PE. Target recognition and visual maps in the thalamus of achiasmatic dogs. Nature. 1994; 367:637–639. [PubMed: 8107846]

Yacoub E, Shmuel A, Logothetis N, Uğurbil K. Robust detection of ocular dominance columns in humans using Hahn Spin Echo BOLD functional MRI at 7 Tesla. Neuroimage. 2007; 37:1161–1177. [PubMed: 17702606]

Highlights

- Hemifield dominance columns are measured in a participant with achiasma
- 2D SE EPI data are acquired at 7 Tesla with 0.8 mm resolution
- T2-weighted, isotropic sampling with large field of view permits novel applications

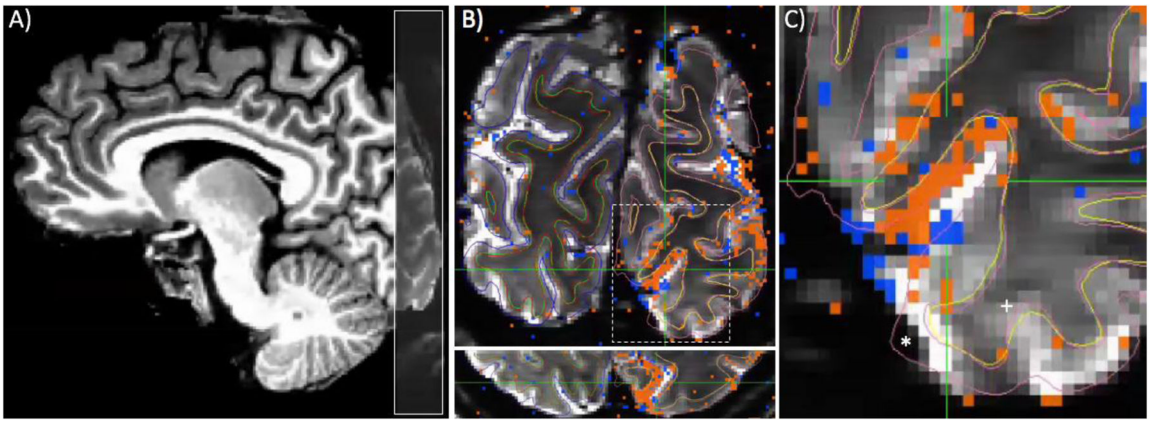

Figure 1.

Functional imaging slice placement, GLM results, and residual distortion. A) Coronal slices (gray overlay) covered a portion of occipital cortex, with 0.8 mm (isotropic) resolution. B) Cortical surfaces (thin lines) and results of GLM (stimulus on minus stimulus off, collapsing across left and right visual hemifield; orange indicates positive fMRI responses; blue, negative) are visualized on functional data after distortion compensation and registration to reference T1-weighted anatomy. In most places, there is excellent agreement between WM/GM/CSF contrast in EPI images and cortical surfaces. C) The crosshairs are centered on a region judged to have good alignment, and included in further analyses. However, large errors are also1 shown, where the GM surface (pink line) from the reference anatomy extends beyond the limit of the tissue seen in EPI data (indicated by *) and where WM surfaces (yellow line) fail to align to evident contrast in EPI data (+). Regions such as this were excluded from further analysis.

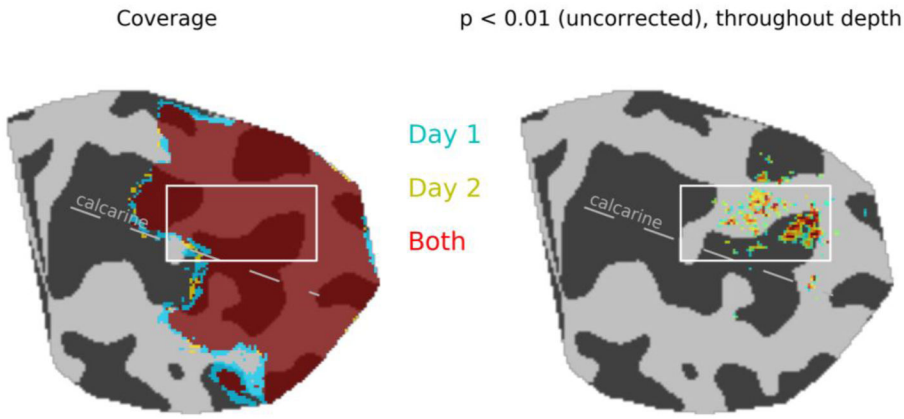

Figure 2.

Coverage and activation maps for two scanning sessions. Average slice placement was slightly more posterior on Day 2, but functional responses in the posterior half of the calcarine were sampled on both days (left panel). Stringent inclusion criteria of individual voxel modulation with $F_{2,1199} > 4.609$, $p < 0.01$ at all cortical depths for voxels with a volume of 0.5-mm^3 resulted in exclusion of regions of the lower bank of the calcarine sulcus, where signal distortion was greatest, from further analysis (right panel). White box indicates regions where data are shown in subsequent figures.

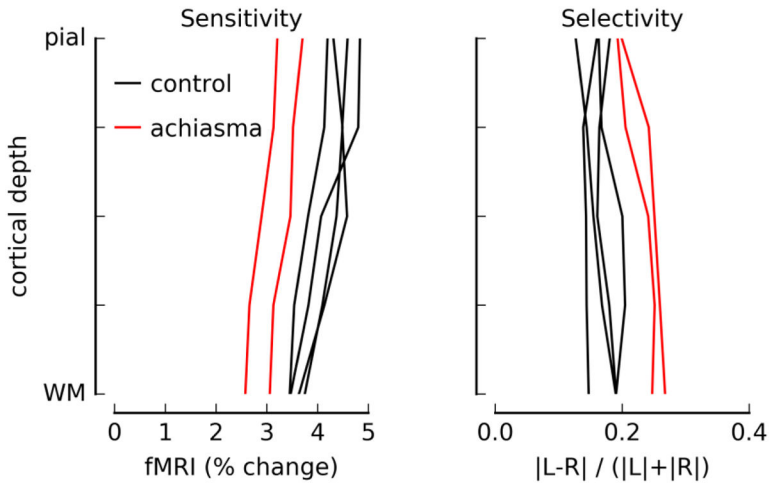

Figure 3.

Sensitivity and selectivity profiles for regions of V1 where responses were strong and EPI/T_1 (functional → anatomical) alignment was good. Sensitivity was computed as the average of the absolute values of the modulation in response to left and right hemifield checkerboard presentations (average magnitude of beta weights in GLM). Selectivity was defined as the difference in beta weights, divided by the sensitivity, with a positive number indicating a stronger response to stimuli in the left visual field. For this plot, the absolute value at each vertex/depth was taken before averaging. Data for the achiasmic participant (two different scanning sessions) are plotted in red; data for two control participants (two scanning sessions, each) are plotted in black.

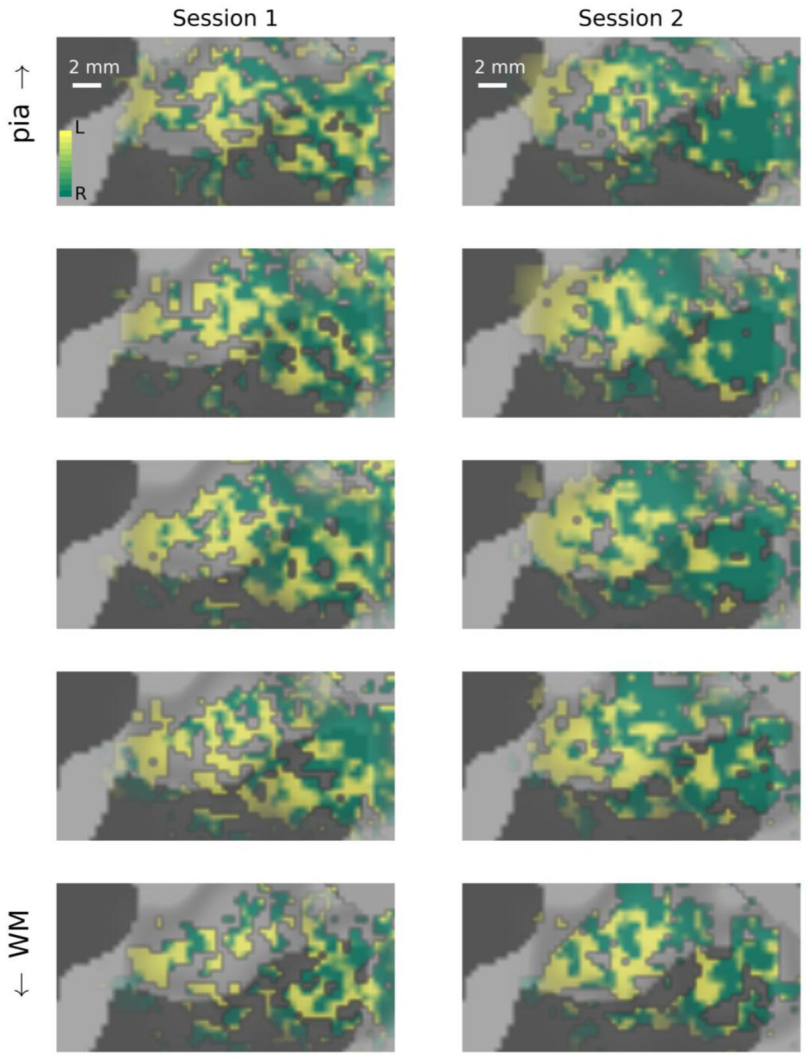

Figure 4.

Visualization of left and right hemifield responses at multiple depth samples in a patch of right V1 located on the dorsal side of the calcarine sulcus (white box, Fig. 2). Left column: data from Day 1; right column: data from Day 2. In each column, data are visualized on flattened surface patches spaced evenly between the white matter (WM, bottom row) and pial surface (pia, top row). Surface vertices at which functional responses were dominated by stimuli presented to the left visual hemifield are shown in green; right visual hemifield dominance is indicated by yellow; saturation indicates degree of dominance (fully saturated colors indicate responses that are 10% larger for one hemifield than the other).

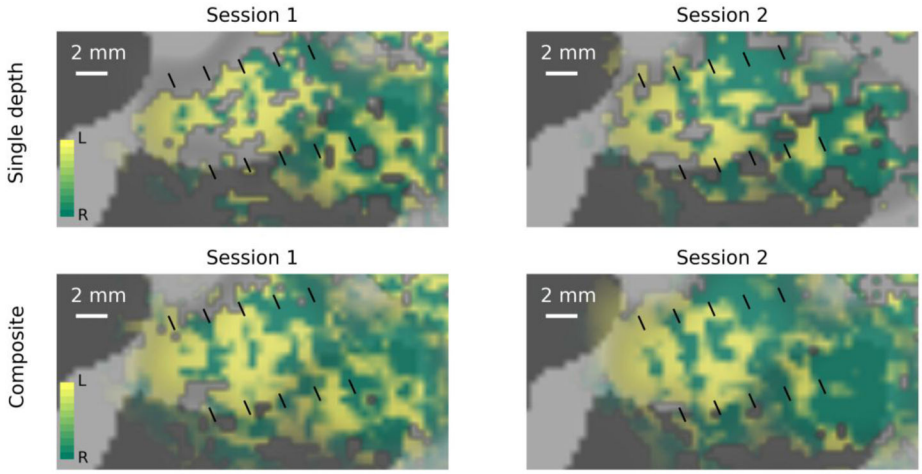

Figure 5.

Visualization of left- vs right-hemifield selectivity in the achiasmic participant. Surface vertices at which functional responses were dominated by stimuli presented to the left visual hemifield are shown in green; right visual hemifield dominance is indicated by yellow; saturation indicates degree of dominance (fully saturated colors indicate responses that are 10% larger for one hemifield than the other). Black fiducial lines mark identical locations on cortex in each panel. Top panel: data sampled at a single depth in the middle of the parenchyma. Bottom panels: composite images formed as weighted sums of the data from all depths, with strong weight given to regions with more power in a 2–3 cyc/mm frequency band.